Supporting Information for

Composition-defined Nanosized Assemblies that Contain Heterometallic Early 4d/5d-Transition-Metals

Masanori Wakizaka, Takane Imaoka,* and Kimihisa Yamamoto*

Laboratory for Chemistry and Life Science Institute of Innovative Research,

Tokyo Institute of Technology, Yokohama 226-8503, Japan

Correspondence and requests for materials should be addressed to K.Y.

E-mail: yamamoto@res.titech.ac.jp

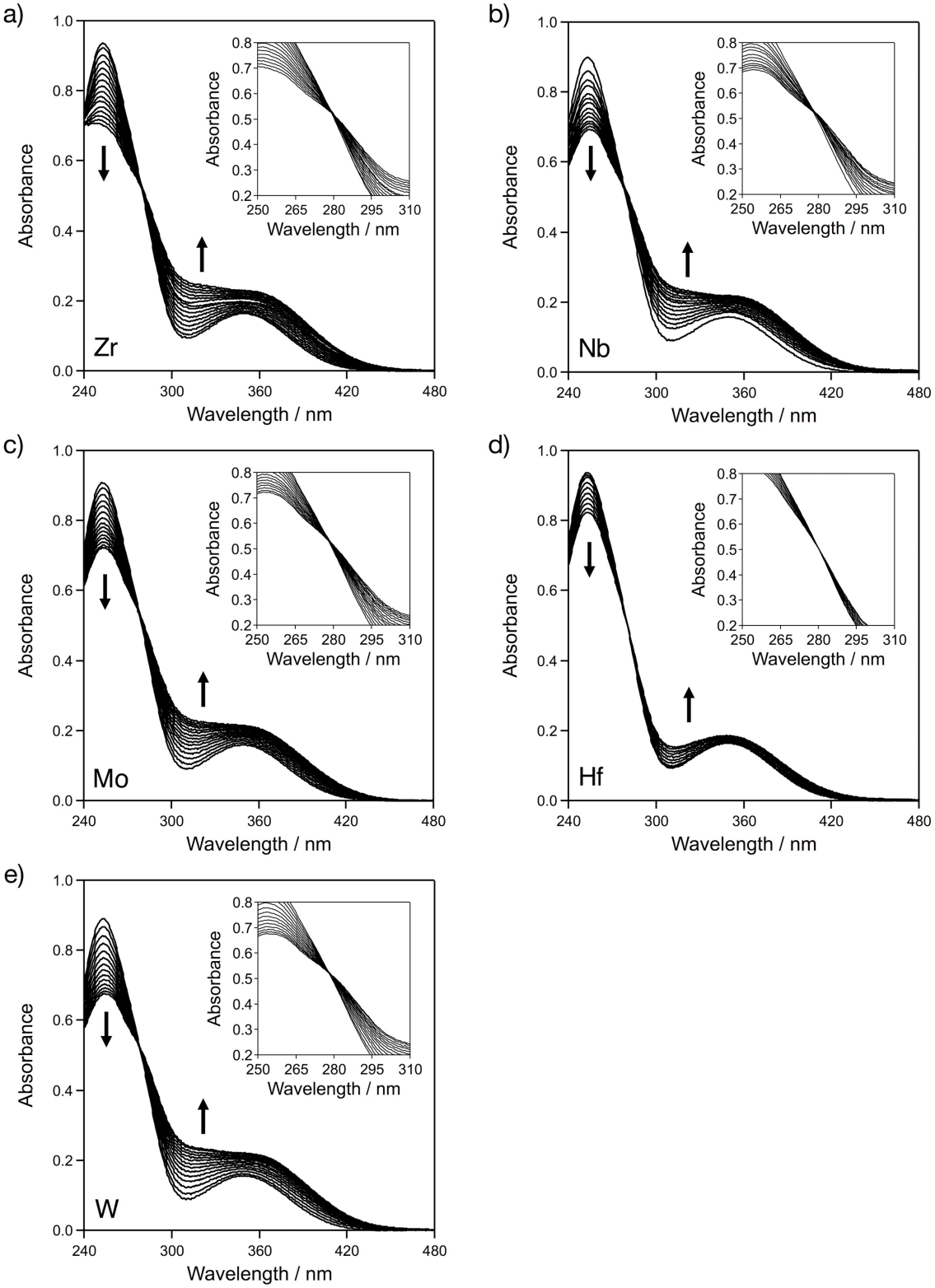

Figure S1. Full range (240–480 nm) UV-vis spectral change of TPM-DPAG1 in CH_2Cl_2/THF = 2/1(*v*/*v*) upon the additions of a) $ZrCl_4$ (0, 6, 12, 18, 24, 30, 36, 42, 48, 54, 60, 66, 72, 78, 84, and 90 eq.), b) $NbCl_5$ (0, 0.5, 1, 1.5, 2, 2.5, 3, 3.5, 4, 4.5, 5, 5.5, 6, and 6.5 eq.), c) $MoCl_5$ (0, 1, 2, 3, 4, 5, 6, 7, 8, 9, 10, 11, 12, 13, and 14 eq.), d) $HfCl_4$ (0, 12, 24, 36, 48, 60, 72, 84, 96, and 108 eq.), and e) WCl_6 (0, 0.5, 1, 1.5, 2, 2.5, 3, 3.5, 4, 4.5, 5, 5.5, 6, 6.5 eq.) in the presence of HMPA (300 eq.) under an atmosphere of N_2 at 245 K. The inserts are magnifications around the isosbestic point.

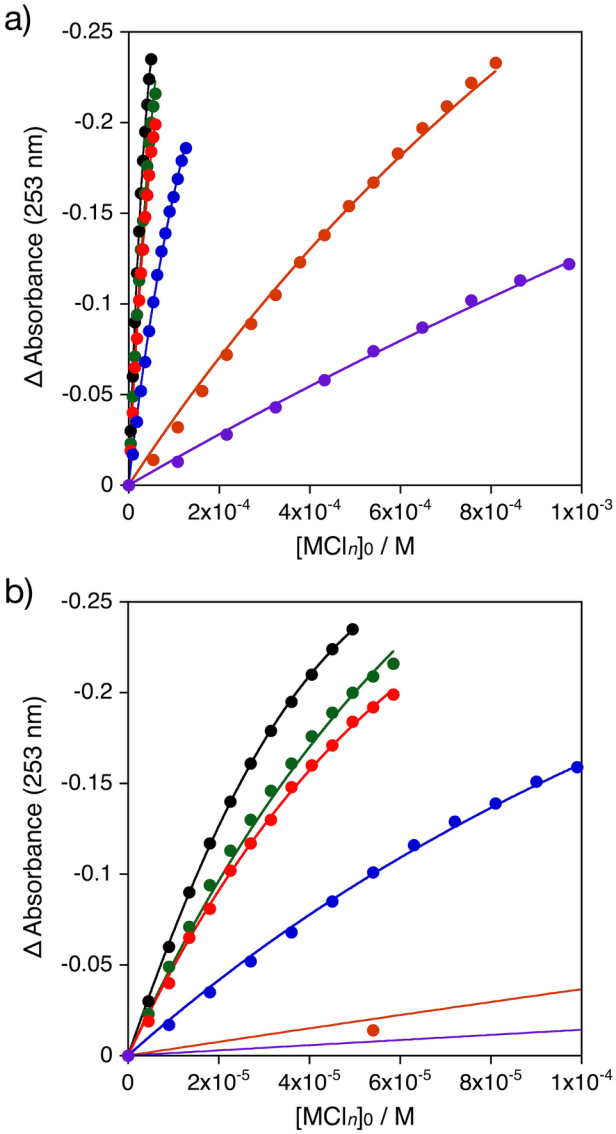

Figure S2. a) Full range (~1 × 10^{-3} M) and b) magnification (~1 × 10^{-4} M) of the titration and fitting curves of TPM-DPAG1 with $TaCl_5$ (black circles and line), WCl_6 (green circles and line), $NbCl_5$ (red circles and line), $MoCl_5$ (blue circles and line), $ZrCl_4$ (orange circles and line), and $HfCl_4$ (purple circles and line) in CH_2Cl_2/THF = 2/1(*v*/*v*) in the presence of HMPA (300 eq.) under an atmosphere of N_2 at 245 K.

Equation S1. K values were estimated by the following equations, wherein $[H]_0$, $[G]_0$, ΔA_{obs}, b, and $\Delta\varepsilon$ refer to the initial concentration of the imines in TPM-DPAG1, the initial concentration of the metal chlorides, the observed differential absorbance, the optical path (1.0 cm), and the differential molar extinction coefficient of the complexes and TPM-DPAG1, respectively.[S1]

$$\Delta A_{obs} = \frac{b\Delta\varepsilon}{2K}\left(X - \{X^2 - 4K^2[H]_0[G]_0\}^{1/2}\right)$$

$$X = 1 + K[H]_0 + K[G]_0$$

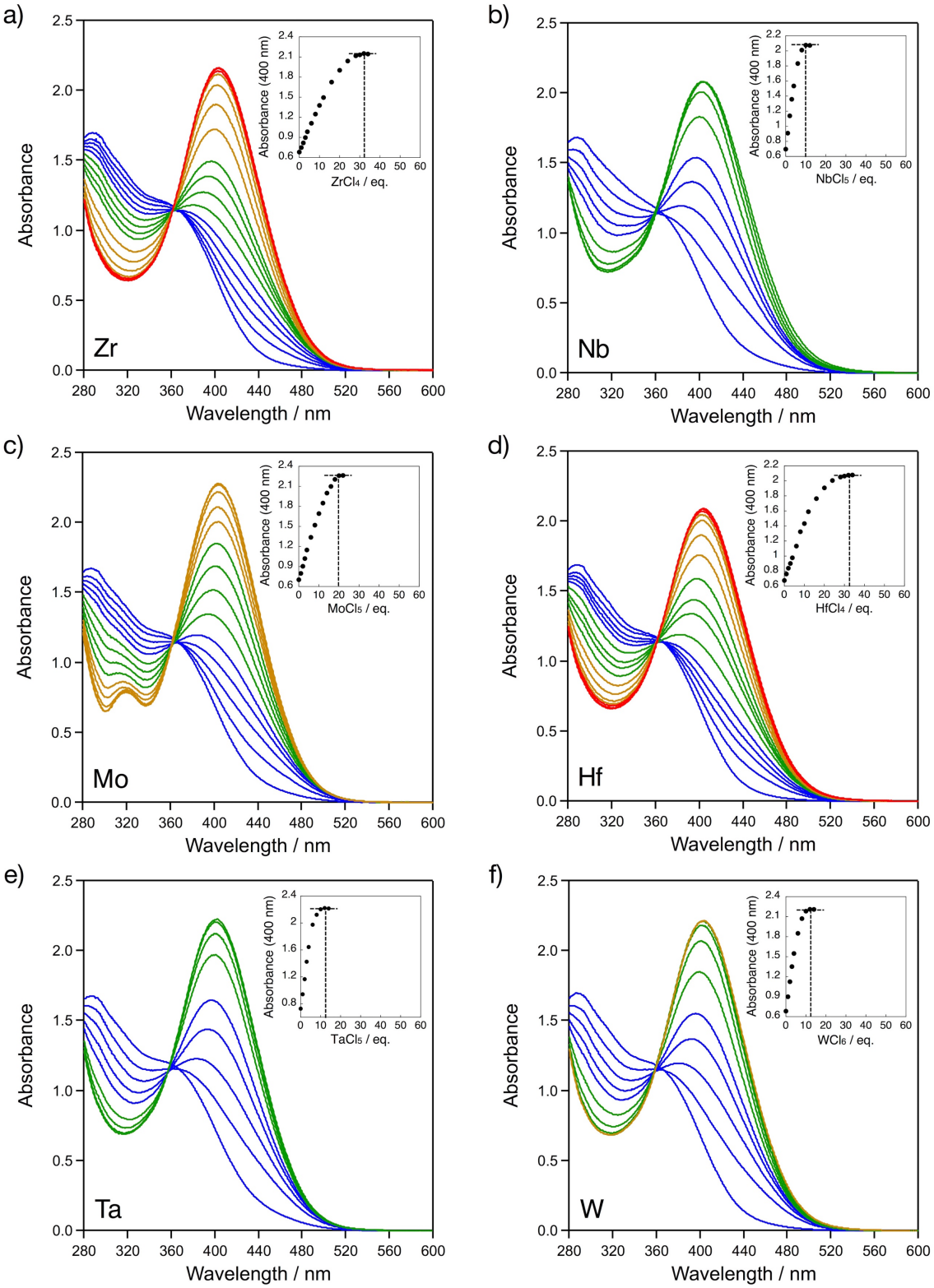

Figure S3. UV-vis spectral change of TPM-DPAG4 in CH_2Cl_2/THF = 2/1(*v*/*v*) upon the additions of a) $ZrCl_4$ (0, 1, 2, 3, 4, 6, 8, 10, 12, 16, 20, 24, 28, 30, 32, and 34 eq.), b) $NbCl_5$ (0, 1, 2, 3, 4, 6, 8, 10, and 12 eq.), c) $MoCl_5$ (0, 1, 2, 3, 4, 6, 8, 10, 12, 14, 16, 18, 20, and 22 eq.), d) $HfCl_4$ (0, 1, 2, 3, 4, 6, 8, 10, 12, 16, 20, 24, 28, 30, 32, and 34 eq.), e) $TaCl_5$ (0, 1, 2, 3, 4, 6, 8, 10, 12, 14 eq.), and f) WCl_6 (0, 1, 2, 3, 4, 6, 8, 10, 12, 14 eq.), under an atmosphere of N_2 at 245 K.

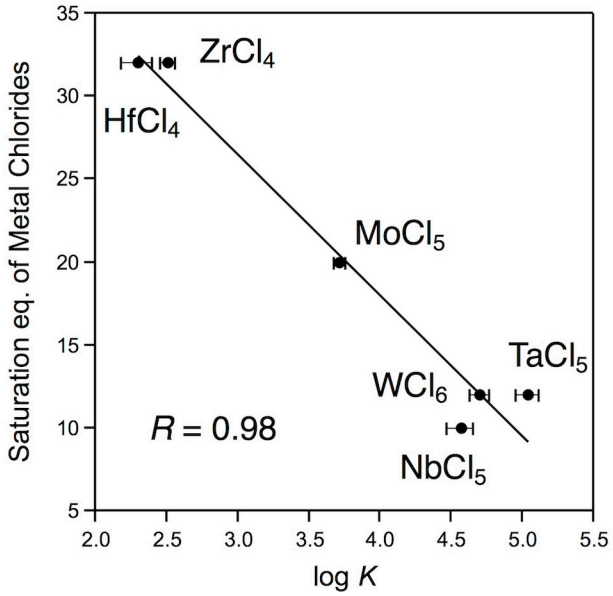

Figure S4. Relationship between log *K* and the saturation equivalents of TPM-DPAG4 and metal chlorides ($R = 0.98$).

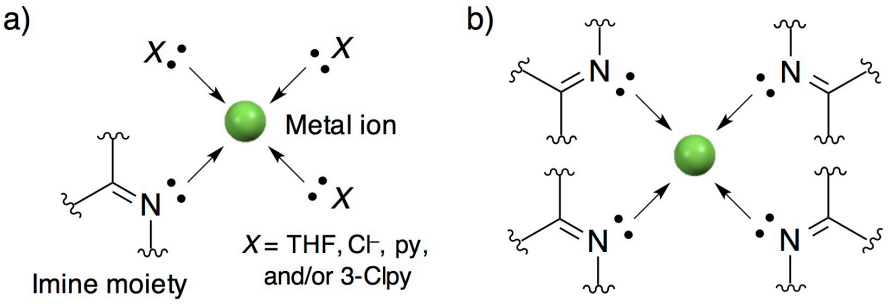

Figure S5. Representative structural illustration of a) a monodentate (stoichiometric coordination) mode, and b) a multidentate mode between imine moieties in a DPA dendrimer and a metal ion in solution.

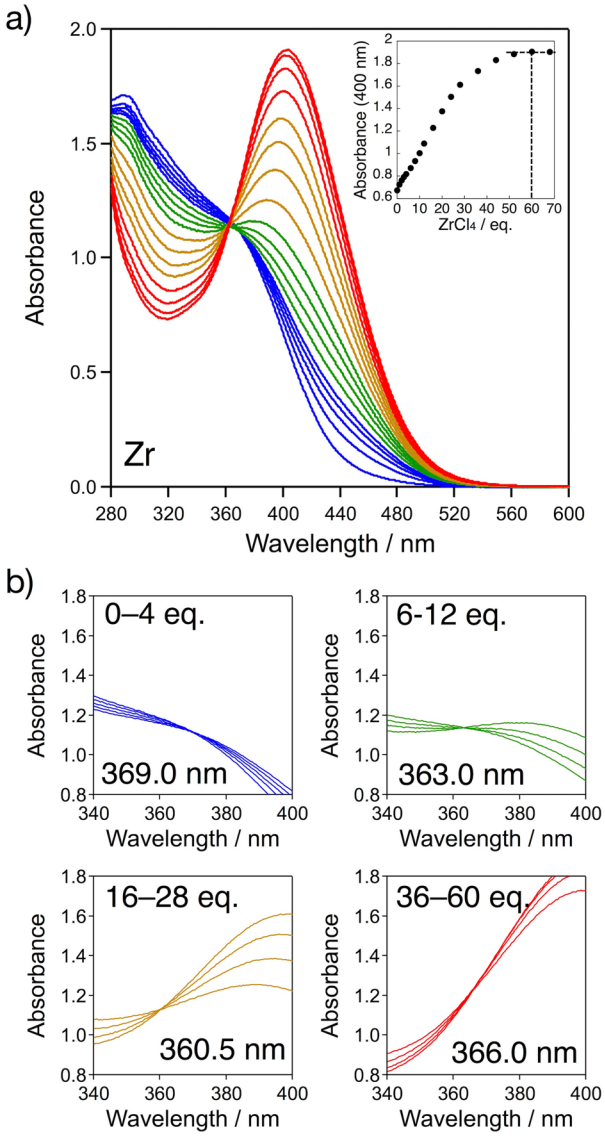

Figure S6. a) Full range (280–600 nm) and b) magnifications around the isosbestic points (340–400 nm) of the UV-vis spectral change of TPM-DPAG4 in CH_2Cl_2/THF = 2/1(*v*/*v*) upon the addition of $ZrCl_4$ (0, 1, 2, 3, and 4 eq.; blue lines), (6, 8, 10, and 12 eq.; green lines), (16, 20, 24, and 28 eq.; orange lines), and (36, 44, 52, and 60 eq.; red lines) in the presence of py (14 eq.) and 3-Clpy (240 eq.), under an atmosphere of N_2 at 245 K.

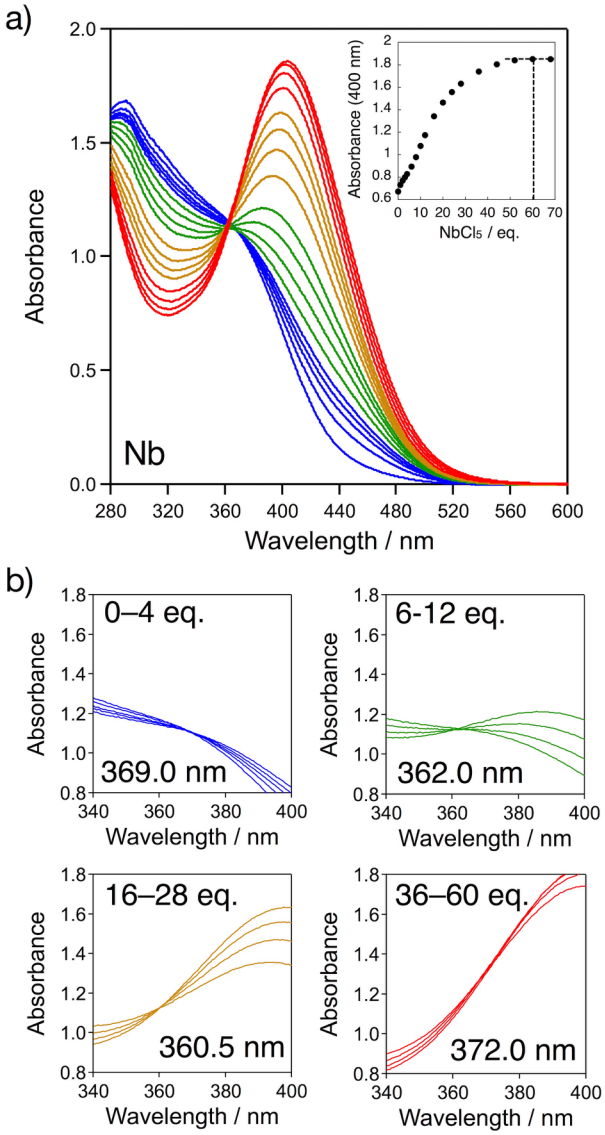

Figure S7. a) Full range (280–600 nm) and b) magnifications around the isosbestic points (340–400 nm) of the UV-vis spectral change of TPM-DPAG4 in CH_2Cl_2/THF = 2/1(*v*/*v*) upon the addition of $NbCl_5$ (0, 1, 2, 3, and 4 eq.; blue lines), (6, 8, 10, and 12 eq.; green lines), (16, 20, 24, and 28 eq.; orange lines), and (36, 44, 52, and 60 eq.; red lines) in the presence of py (20 eq.) and 3-Clpy (600 eq.), under an atmosphere of N_2 at 245 K.

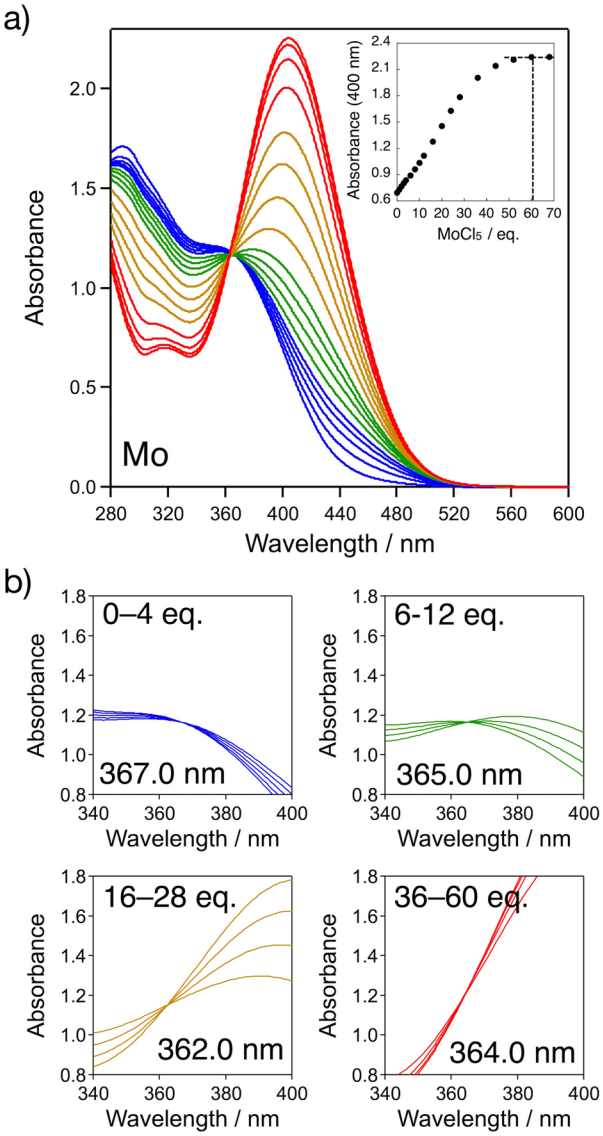

Figure S8. a) Full range (280–600 nm) and b) magnifications around the isosbestic points (340–400 nm) of the UV-vis spectral change of TPM-DPAG4 in CH_2Cl_2/THF = 2/1(*v*/*v*) upon the addition of $MoCl_5$ (0, 1, 2, 3, and 4 eq.; blue lines), (6, 8, 10, and 12 eq.; green lines), (16, 20, 24, and 28 eq.; orange lines), and (36, 44, 52, and 60 eq.; red lines) in the presence of py (4 eq.) and 3-Clpy (40 eq.), under an atmosphere of N_2 at 245 K.

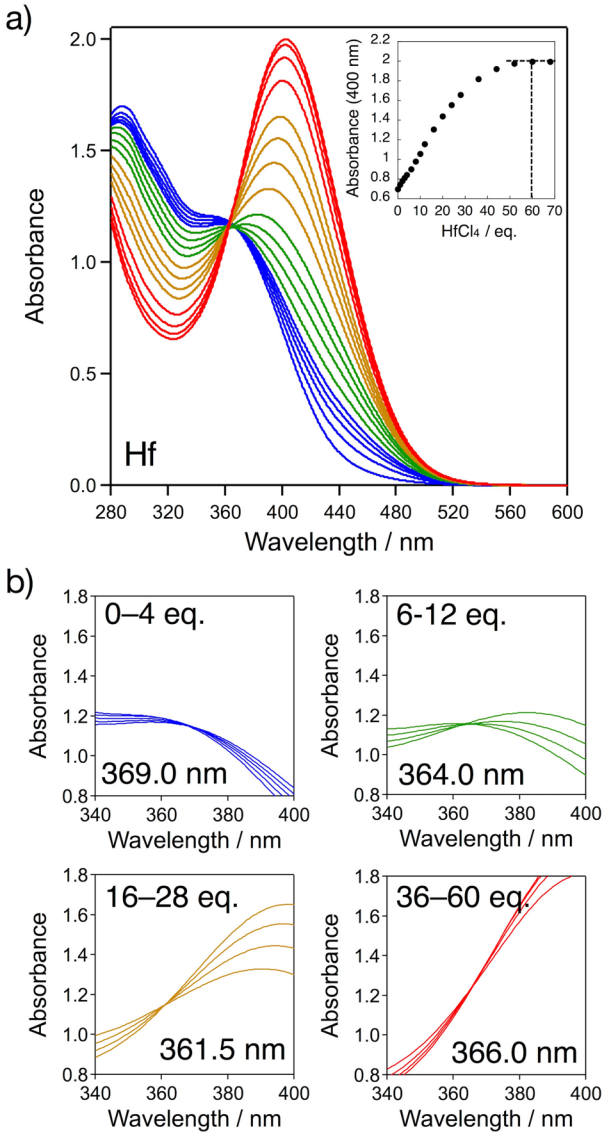

Figure S9. a) Full range (280–600 nm) and b) magnifications around the isosbestic points (340–400 nm) of the UV-vis spectral change of TPM-DPAG4 in CH_2Cl_2/THF = 2/1(*v*/*v*) upon the addition of $HfCl_4$ (0, 1, 2, 3, and 4 eq.; blue lines), (6, 8, 10, and 12 eq.; green lines), (16, 20, 24, and 28 eq.; orange lines), and (36, 44, 52, and 60 eq.; red lines) in the presence of py (12 eq.) and 3-Clpy (210 eq.), under an atmosphere of N_2 at 245 K.

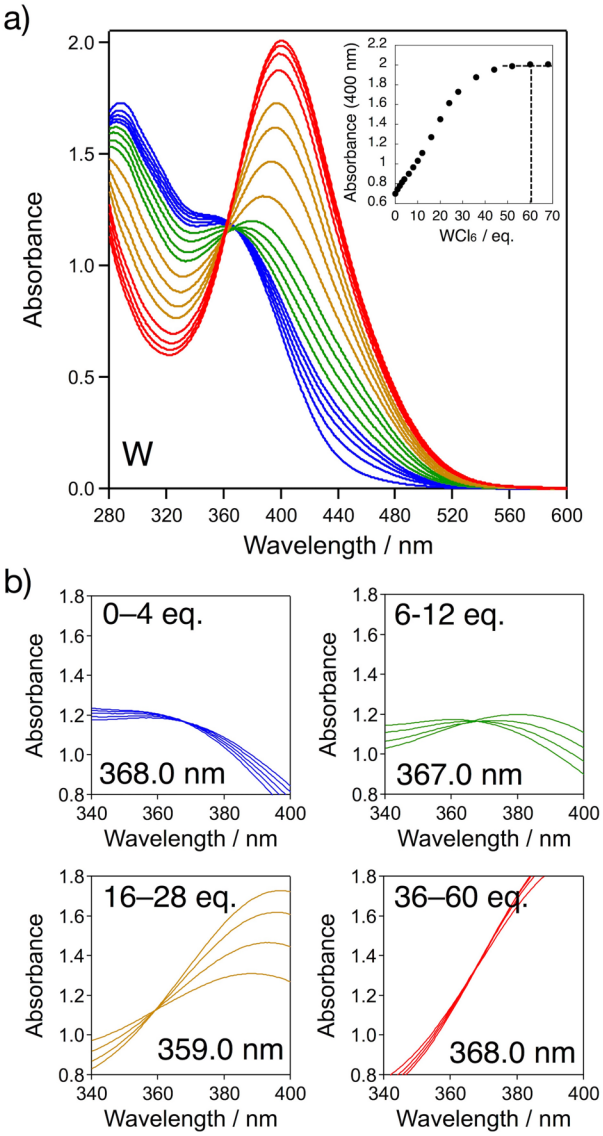

Figure S10. a) Full range (280–600 nm) and b) magnifications around the isosbestic points (340–400 nm) of the UV-vis spectral change of TPM-DPAG4 in CH_2Cl_2/THF = 2/1(*v*/*v*) upon the addition of WCl_6 (0, 1, 2, 3, and 4 eq.; blue lines), (6, 8, 10, and 12 eq.; green lines), (16, 20, 24, and 28 eq.; orange lines), and (36, 44, 52, and 60 eq.; red lines) in the presence of py (40 eq.) and 3-Clpy (900 eq.), under an atmosphere of N_2 at 245 K.

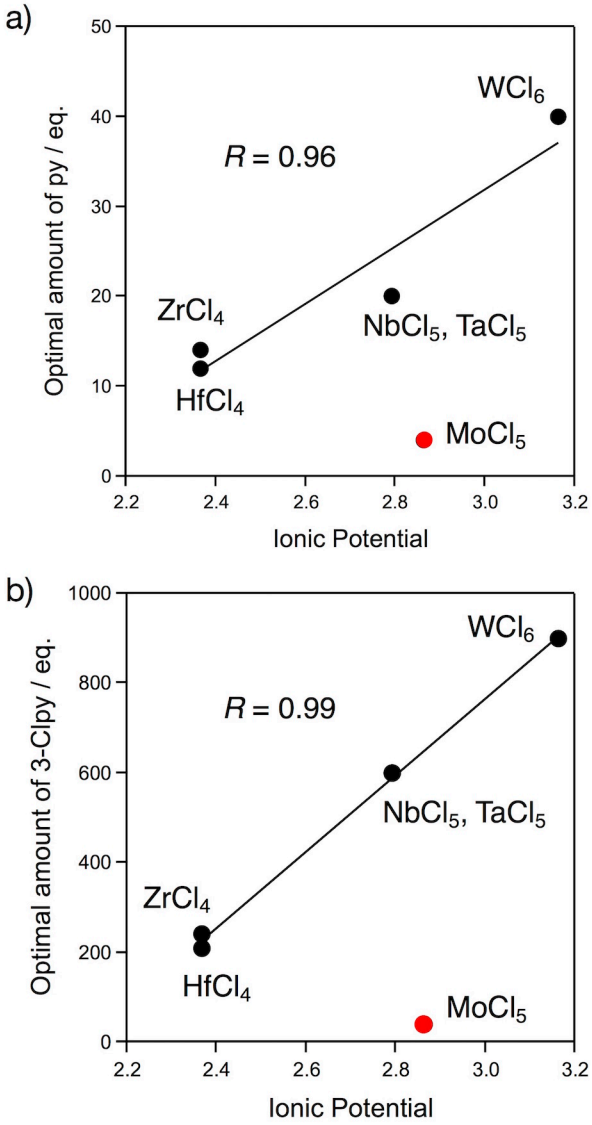

Figure S11. Relationship between the ionic potential of Zr^{IV}, Nb^{V}, Hf^{IV}, Ta^{V}, W^{VI} (black circles), and Mo^{V} (red circle) and the optimal amount of a) py (R = 0.96) and b) 3-Clpy (R = 0.99) with the approximate line estimated except for the point of $MoCl_5$.

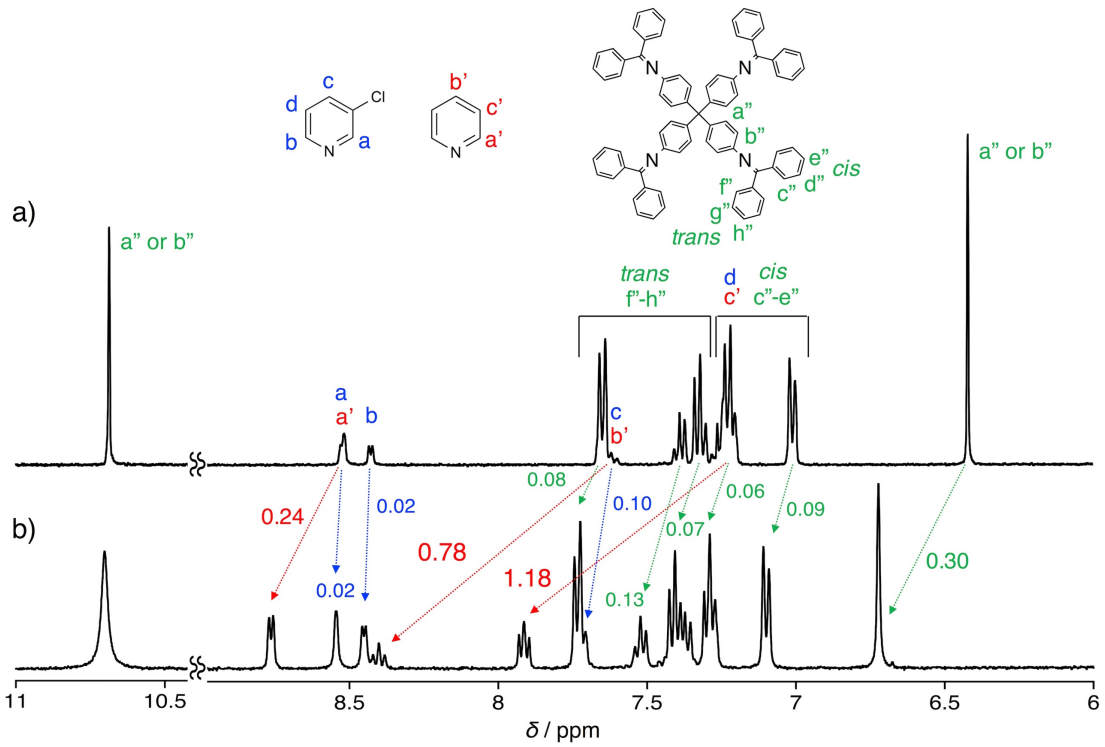

Figure S12. ^{1}H NMR spectra of a) TPM-DPAG1 with py (1 eq.) and 3-Clpy (1 eq.), as well as b) in the presence of $TaCl_5$ (2 eq.) in CD_2Cl_2/THF-d_8 = 2/1(*v*/*v*), under an atmosphere of N_2 at room temperature.

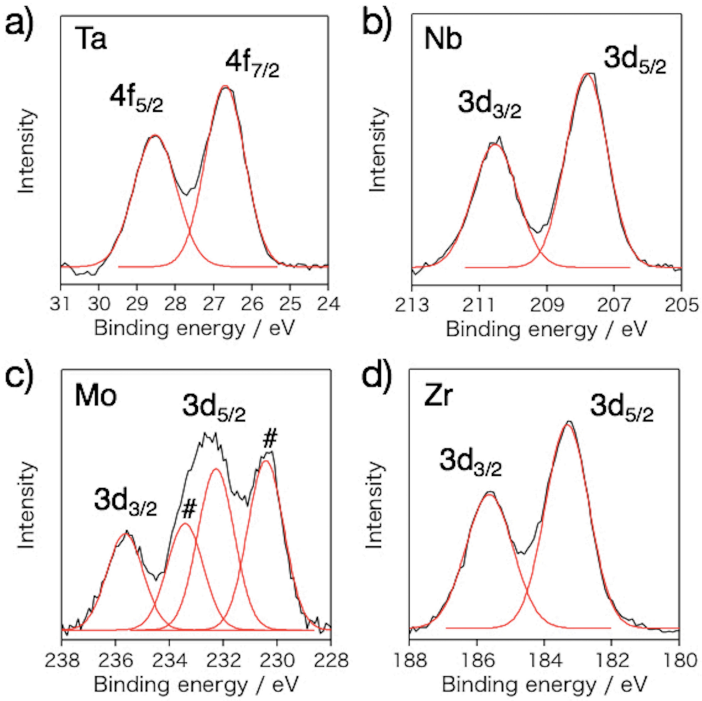

Figure S13. XPS spectra of the crude mixture composed of $M^{n+}Cl_n$ (M = Ta^V, Nb^V, Mo^{V+}, Zr^{IV}) on the GMC in the range around the binding energies of a) Ta, b) Nb, c) Mo, and d) Zr with fitting curves. The marked peaks (#) of 230.4 and 233.4 eV indicate reductive species of Mo, which was generated during the mixing.

Table S1. Summary of XPS data

Region	Binding energy / eV	Sum of areas (A)	Mole ratio $A_M{}^a/A_{Ta}{}^a \times A_{Ta}{}^b/A_M{}^b \times n^d$
Ta $4f_{7/2}{}^a$	26.5	1126.6±54.2	1
Ta $4f_{5/2}{}^a$	28.3		
Nb $3d_{5/2}{}^a$	207.8	3178.2±119.1	2.6±0.2
Nb $3d_{3/2}{}^a$	210.6		
Mo $3d_{5/2}{}^a$	232.2	6862.1±114.3	4.1±0.2
Mo $3d_{3/2}{}^a$	235.5		
Zr $3d_{5/2}{}^a$	183.4	7442.1±74.0	8.9±0.4
Zr $3d_{3/2}{}^a$	185.7		
Ta $4f_{7/2}{}^b$	26.7	11687.2±103.4	1^d
Ta $4f_{5/2}{}^b$	28.5		
Nb $3d_{5/2}{}^b$	207.8	13969.0±88.6	1.12^d
Nb $3d_{3/2}{}^b$	210.5		
Mo $3d_{5/2}{}^b$	232.3	17944.8±236.5^c	1.03^d
Mo $3d_{3/2}{}^b$	235.7		
Zr $3d_{5/2}{}^b$	183.3	9775.6±32.7	1.13^d
Zr $3d_{3/2}{}^b$	185.6		

^{a} in the assembly composed of $M^{n+}Cl_n$ (M = Ta^V, Nb^V, Mo^V, Zr^{IV}) and TPM-DPAG4 on the GMC. ^{b} in the crude mixture composed of $M^{n+}Cl_n$ (M = Ta^V, Nb^V, Mo^V, Zr^{IV}) on the GMC. ^{c} including the areas of reductive species. ^{d} n refers mole ratio in the crude mixture.

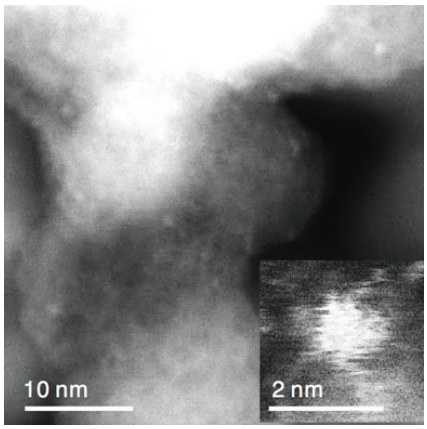

Figure S14. HAADF-STEM image in the heterometallic assemblies composed of $M^{n+}Cl_n$ (M = Ta^{V}, Nb^{V}, Mo^{V}, Zr^{IV}) and TPM-DPAG4 on the GMC. The inset is a high-resolution image.

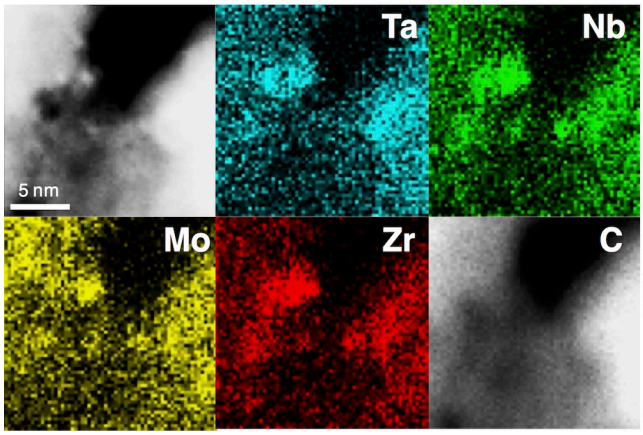

Figure S15. Wide range HAADF-STEM and EDS mapping images of Ta (light blue), Nb (green), Mo (yellow), Zr (red), and C (grey) on the assemblies composed of $M^{n+}Cl_n$ (M = Ta^{V}, Nb^{V}, Mo^{V}, Zr^{IV}) and TPM-DPAG4 on the GMC.

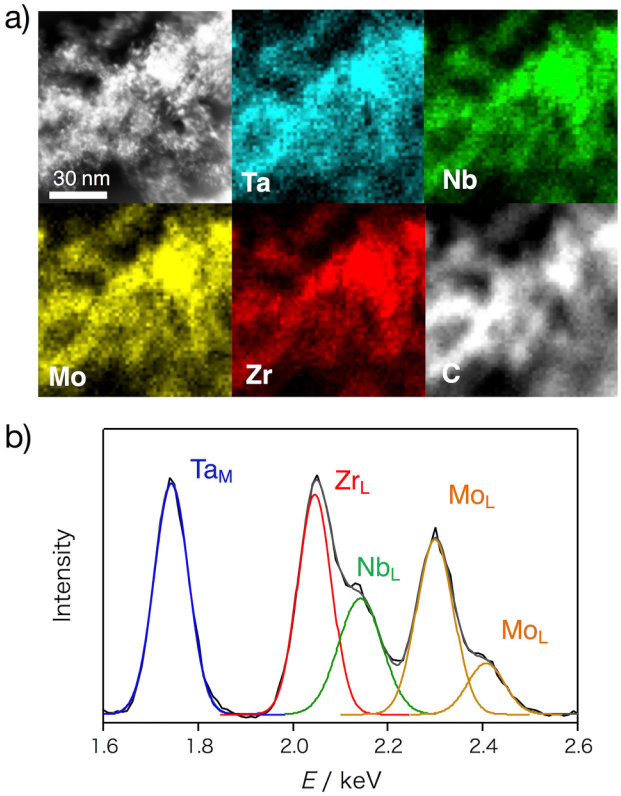

Figure S16. a) HAADF-STEM and EDS mapping images of Ta (light blue), Nb (green), Mo (yellow), Zr (red), and C (grey); b) EDS spectrum of the crude mixture composed of $M^{n+}Cl_n$ (M = Ta^V, Nb^V, Mo^V, Zr^{IV}) on the GMC with fitting curves.

Table S2. Summary of EDS data

Metal	*E* / keV	Area (*A*)	Mole ratio $A_M{}^a/A_{Ta}{}^a \times A_{Ta}{}^b/A_M{}^b \times n^c$
Ta[a]	1.74	8.41±0.29	1
Nb[a]	2.15	4.47±0.37	1.7±0.2
Mo[a]	2.30, 2.40	7.85±0.34, 1.95±0.34	4.4±0.3
Zr[a]	2.05	8.18±0.34	8.3±0.5
Ta[b]	1.74	476.46±3.37	1[c]
Nb[b]	2.15	304.25±4.38	2.0[c]
Mo[b]	2.30, 2.40	388.41±3.66, 113.70±3.66	4.0[c]
Zr[b]	2.05	444.50±3.99	8.0[c]

[a] in the assembly composed of $M^{n+}Cl_n$ (M = Ta^V, Nb^V, Mo^V, Zr^{IV}) and TPM-DPAG4 on the GMC. [b] in the crude mixture composed of $M^{n+}Cl_n$ (M = Ta^V, Nb^V, Mo^V, Zr^{IV}) on the GMC. [c] *n* refers mole ratio in the crude mixture.

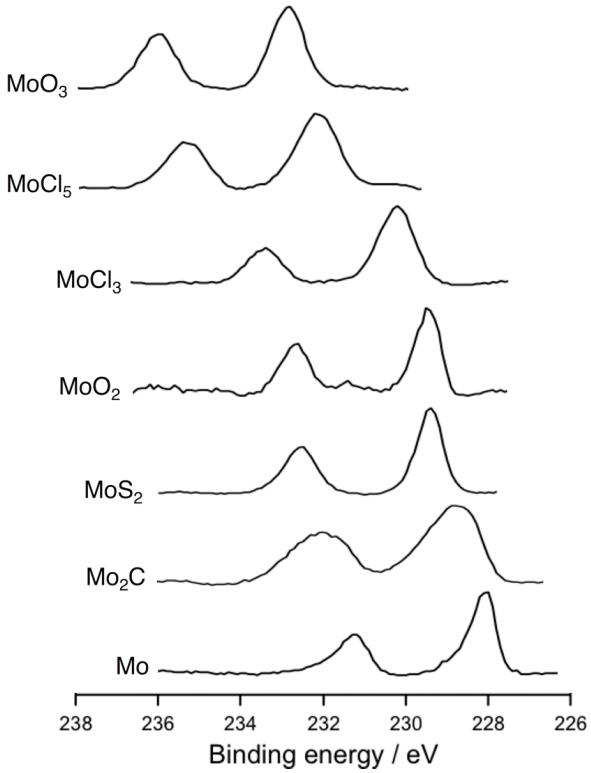

Figure S17. XPS spectra of MoO_3, $MoCl_5$, $MoCl_3$, MoO_2, MoS_2, Mo_2C, and Mo on GMC. Binding energies were calibrated for C1s of GMC (284.5 eV).

Table S3. Summary of XPS data for Mo samples

Sample	Binding energy / eV[a]	
	Mo $3d_{5/2}$	Mo $3d_{3/2}$
MoO_3	232.9	236.0
$MoCl_5$	232.1	235.3
$MoCl_3$	230.2	233.4
MoO_2	229.5	232.7
MoS_2	229.4	232.6
Mo_2C	228.9	232.1
Mo	228.2	231.3

[a] Calibrated for C1s of GMC (284.5 eV)

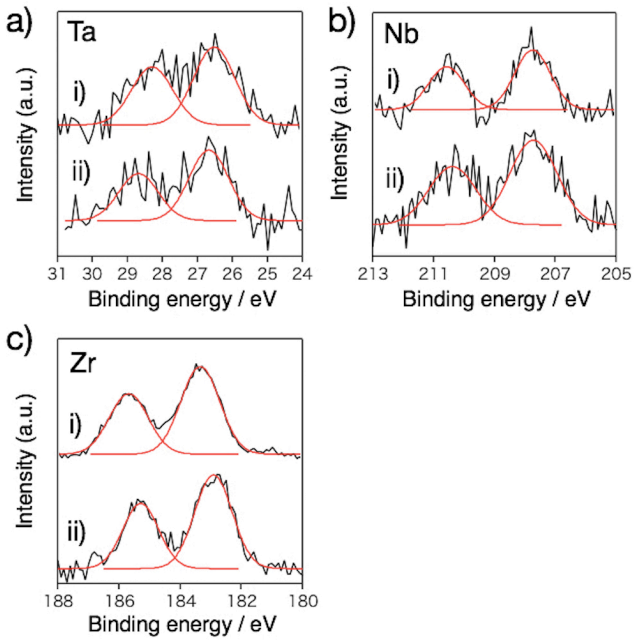

Figure S18. XPS spectra of i) the heterometallic assembly composed of $M^{n+}Cl_n$ (M = Ta^{V}, Nb^{V}, Mo^{V}, Zr^{IV}) and TPM-DPAG4 on GMC and ii) the product after the reaction under an atmosphere of H_2 at 773 K. The spectra cover the range of binding energies of a) Ta, b) Nb, and c) Zr with fitting curves.

Table S4. Summary of XPS data for the product[a]

Region	Binding energy / eV
Ta $4f_{7/2}$	26.7
Ta $4f_{5/2}$	28.7
Nb $3d_{5/2}$	207.7
Nb $3d_{3/2}$	210.4
Mo $3d_{5/2}$	229.5, 232.9
Mo $3d_{3/2}$	232.9, 236.1
Zr $3d_{5/2}$	182.9
Zr $3d_{3/2}$	185.3

[a] the product of the assembly composed of $M^{n+}Cl_n$ (M = Ta^{V}, Nb^{V}, Mo^{V}, Zr^{IV}) and TPM-DPAG4 on the GMC after the reaction under an atmosphere of H_2 at 773 K.

References

S1. K. A. Connors, *Binding constants: the measurements of molecular complex stability*, John Wiley + Sons, 1987.